ELSEVIER

Astroparticle Physics 16 (2001) 75–96

Astroparticle Physics

www.elsevier.com/locate/astropart

Further studies of the OMNIS supernova neutrino observatory: optimisation of detector configuration and possible extension to solar neutrinos

Peter F. Smith *

Rutherford Appleton Laboratory, Department of Particle Physics, Chilton, Oxfordshire OX11 0QX, UK

Received 13 November 2000; received in revised form 2 January 2001; accepted 11 January 2001

Abstract

The basic design principles and earlier origins of OMNIS (Observatory for Multiflavour Neutrino Interactions from Supernovae) have been described in a previous paper [Astropart. Phys. 8 (1997) 27]. Its purpose would be to record a large number of mu and tau neutrinos from a supernova burst, complementing other world detectors which observe mainly electron antineutrinos. This would enable a cosmologically significant neutrino mass to be measured or definitely excluded by the arrival time profile. The detector is based on neutral current excitation of lead and iron target nuclei followed by release of neutrons. Further studies by Fuller et al. [Phys. Rev. D59 (1999) 085005] have shown that a distinctive two-neutron signal will result from an MSW transition between $\nu_{\mu,\tau}$ and ν_e in the supernova, thus adding further physics capability to OMNIS. In this paper we summarise the published neutron production estimates for different targets, with and without mixing, and discuss the results of simulations of a range of target/detector configurations, with the objective of optimising the single and double neutron signals from a given target mass. Discussions are included of the choice of neutron detection method, and the effect of neutron and gamma backgrounds. It is further proposed that OMNIS detector modules might be designed to include real-time solar neutrino spectroscopy using the nuclear excitation principle devised by Raghavan [Phys. Rev. Lett. 78 (1997) 3618].

PACS: 97.60B; 13.15; 14.60; 29.40; 94.40T; 98.50
Keywords: Neutrinos; Neutrino oscillations; Neutrino mass; Supernova; Detectors

1. Introduction

OMNIS (observatory for multiflavour neutrino interactions from supernovae) is a proposed astrophysical neutrino observatory with high efficiency for the detection of neutrinos above 10 MeV in momentum. [1] It is based primarily on the neutral or charged current excitation of nuclei, releasing neutrons of MeV-range energy which escape from the target to be thermalised and absorbed in nearby neutron detectors. The energy dependence of this process makes it uniquely

* Tel.: +44-1235-445463; fax: +44-1235-446733.
E-mail address: p.f.smith@rl.ac.uk (P.F. Smith).

[1] Units in this paper are based on $\hbar = c = 1$, so that energy, momentum, mass, are all expressed in eV.

0927-6505/01/$ - see front matter
PII: S0927-6505(01)00104-9

suitable for the observation of the time profile of mu and tau neutrinos from a Galactic supernova burst, and hence to observe time-of-flight differences arising from a cosmologically significant neutrino mass, or flavour mixing effects from much smaller masses.

For a given incident energy, nuclear excitation has a cross-section typically an order of magnitude higher than that of the commonly used ν_e–e detection process, being $\sim 10^{-42}$ cm^2 at 30 MeV, subsequently de-exciting with an nucleus-dependent branching ratio to neutrons [1]. In addition, the unusual feature of transporting the signal by neutron scattering provides a geometric freedom which allows events from a large target mass to be registered by a relatively small detector mass. These two features allow a considerable reduction in size and cost compared with supernova detectors based on conventional liquid scintillator and water Cerenkov detectors.

The evolution of OMNIS was described in a previous paper [2]. An earlier proposal by Cline et al. [3–5] had been based on the use of underground rock as a target, with embedded neutron detectors. More detailed study showed that the use of rock as target had disadvantages both from low neutron production in light elements and inefficient neutron collection due to thermalisation and absorption in the rock itself [2]. This investigation demonstrated that both neutron production and collection could be improved by an order of magnitude by the use of heavier elements, the most suitable from a cost viewpoint being Pb and Fe. Moreover, other theoretical studies [27] summarised below, showed that Pb provides additional signals from charged current interactions which are enhanced by neutrino mixing $(\nu_\tau, \nu_\mu \rightarrow \nu_e)$ in transit or from an MSW transition in the supernova itself. In particular a distinctive two-neutron signal would be seen in Pb, but not in Fe targets. It is the comparison between the neutron time profiles from Pb and Fe targets, combined with the selective response to the heavier flavours ν_τ, ν_μ, which provides the unique multiflavour physics distinguishing the OMNIS concept from previous astrophysical neutrino detectors.

In Section 2, we review published estimates for Galactic supernova rates, time profiles and fluxes, and give tabulated summaries of calculated neutron production rates in relevant target materials. In Section 3, we extend our previous work on neutron collection efficiency from different target materials, leading to some typical generic OMNIS configurations, with estimates of target mass required for a given number of events. Requirements for observation of neutrino mixing effects are discussed in Section 4, in particular the predicted numbers of single and two-neutron events, and the effect of variations in detector + target geometry are calculated. In Section 5, specific examples of typical individual OMNIS modules are shown, with single and two-neutron event numbers with and without mixing.

The possibility of designing an astrophysical neutrino observatory sensitive to more than one type of neutrino source is being considered. The use of Gd-loaded scintillator with Pb and Fe targets for OMNIS allows, in principle, the incorporation of solar neutrino interactions by real time excitation of nuclei (SIREN) based on the recently proposed Gd excitation scheme [6,7]. The Gd and scintillator would be common to both detectors, while the SIREN shielding doubles as the OMNIS target [8,9]. Some design and background problems for this combined scheme are discussed in Section 6.

2. Supernova rates, neutrino burst characteristics

2.1. Galactic supernova rates

The majority of recorded supernovae lie within 4–5 kpc of the sun, those at larger distances (in the Galactic plane) being obscured. This observable region contains only 6–8% of the Galactic star population [10,12,15], so that if this is a representative sample the total supernova rate should be 12–16 times the rate recorded optically.

A number of authors have compared the historical record with various astrophysical estimates of the expected rate [10–13,44]. Although 200 supernova remnants have been recorded in our Galaxy, only the last two millennia provide a sufficiently complete record to estimate the rate [12]. Adding to those listed in Ref. [12] the recently

discovered remnant dated 1320 [14], there are 8–9 type II/Ib supernovae recorded in 2200 years in the local ~7% sample of our Galaxy. This indicates a most probable rate $\sim 6 \pm 1$ per century. This is significantly greater than the more favoured estimates of 3 ± 1 per century from extra-galactic observations. However, reviews of rate estimates based on a variety of astrophysical methods [10,11] show that these can range from 2–10 per century, consistent with the historical record. An additional population of supernovae, optically 'ultra-dim' but producing neutrino bursts, has also been suggested [15].

A recent discussion [13] suggests that the historical rate could be misleadingly high if the Galaxy is not axially symmetric and the solar system may lie in a favoured region. However, this would require that 15–20% of Galactic supernovae occur in the local 7% of stars – a seemingly unlikely spatial bias in view of the fact that this local sample crosses three of the spiral arms. In the absence of local bias, therefore, we can assume the most likely supernova interval for the whole Galaxy to be in the range 14–20 years. This rather long interval emphasises the need for a full range of detectors forming a world supernova watch to extract maximum information from the burst. The role of OMNIS would be to complement other detectors in providing the specialised higher-flavour signals discussed in this paper.

2.2. Time profile of neutrino burst

The basic mechanism of stellar collapse and supernova explosions has been reviewed and summarised by Raffelt [16]. Models differ in detail and are still the subject of theoretical study, but the generic form of the neutrino burst is generally agreed to be as illustrated in Fig. 1 [16,17] which shows luminosity versus time for the three neutrino flavours and their antiparticles.

The expected rate of arrival of events is important for specifying the instrumentation and subdivision of OMNIS, in particular in relation to the efficiency with which the two-neutron mixing signal can be distinguished, as shown in Section 4 below. That the time profile of Fig. 1 is at least approximately correct was shown by the 19 neu-

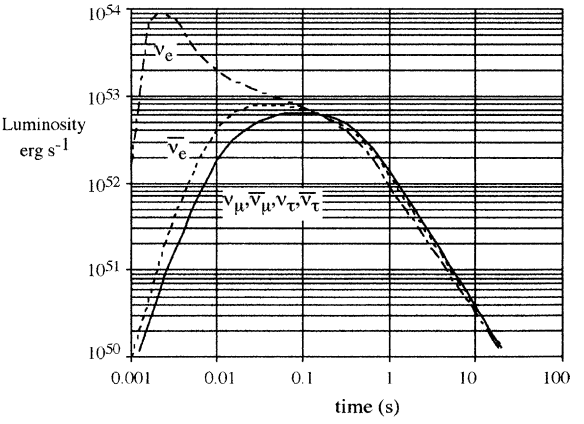

Fig. 1. Generic form of supernova neutrino burst, showing luminosity versus time for the different neutrinos (from [10]).

trino events [13,21,22] seen in the IMB and Kamiokande detectors from supernova 1987a (Fig. 2a). Despite the small number of events, the profile is consistent with the expectation that ~70% of the neutrinos are released in the first 2 s, though the best fit to the integral curve suggests a slightly longer time constant in this case (Fig. 2b). In addition, the number and energy of events is consistent with the expected $\bar{\nu}_e$ flux and temperature [16,22] as noted in Section 2.4.

The existence of a 'cosmologically significant' mass (e.g. 10–100 eV) for one flavour, e.g. ν_τ (in the absence of mixing) would, due to the time of flight difference over the typical 8 kpc distance, produce an observable delay or 'stretching' of the arrival profile of that neutrino, relative to the arrival profile of the lower mass neutrinos. Using the emission profile of Fig. 1, the change in arrival profile of a heavier neutrino is shown in Fig. 3a. The resulting time profile for a zero mass ν_μ and a non-zero mass ν_τ is shown in Fig. 3b. [2] For convenience a 'no-mixing' terminology is used here, in which the weak eigenstates ν_e, ν_μ, ν_τ are also the mass eigenstates. In the presence of mixing the time-of-flight delays would refer to the mass eigenstates ν_1, ν_2, ν_3, which may still be approximately the weak eigenstates if

[2] This supersedes Fig. 3 of [2] which used a simplified exponential time profile to illustrate non-zero mass effects.

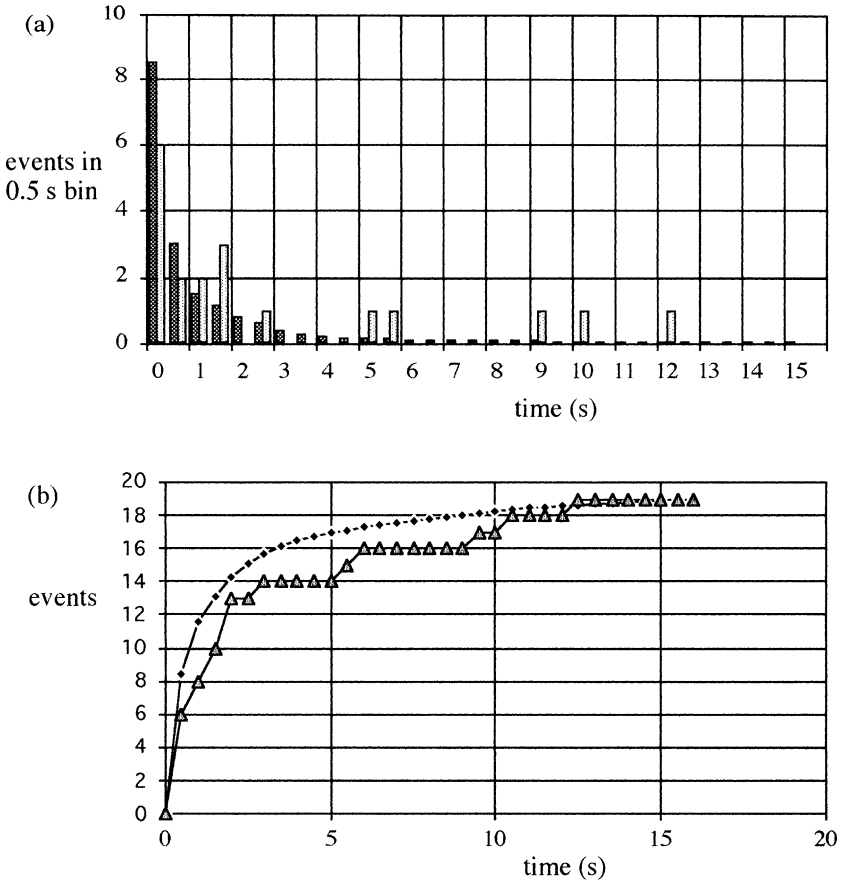

Fig. 2. Electron antineutrino events from supernova 1987a: (a) histogram of observed 19 events (light shading) with profile calculated from Fig. 1 (dark shading); (b) integrals of (a) observed events (triangles) and model prediction (diamonds) for same total.

the mixing angle is small. For large mixing angle the number of events in the heaviest eigenstate remains unchanged, and the time profile analysis is unaffected. The following points arise in the estimation of non-zero mass:

(a) Independently of information from other detectors, the arrival profile could be separated into (eg) two individual components by an iterative analysis for an assumed neutrino temperature.

(b) It is not necessary to use the ν_e or $\bar{\nu}_e$ time profile from other detectors to define the point $t = 0$. Because of the wide range of energies in the burst the additional travel time, given by

$$\Delta t(s) = 0.5\,(R/10\ \text{kpc})(m_\nu/20\ \text{eV})^2 \times (20\ \text{MeV}/E_\nu)^2 \quad (1)$$

is small for the highest energies in the (approximately Dirac) neutrino spectrum, so that non-zero mass causes the time profiles to be 'stretched' rather than delayed and thus remain anchored to the point $t = 0$, as shown by the examples in Fig. 3.

(c) For a τ mass ~25–50 eV the profile distortion is a large effect and would be significant with only ~100 events.

(d) For masses 10–100 eV Monte Carlo simulations indicate that a non-zero mass could be

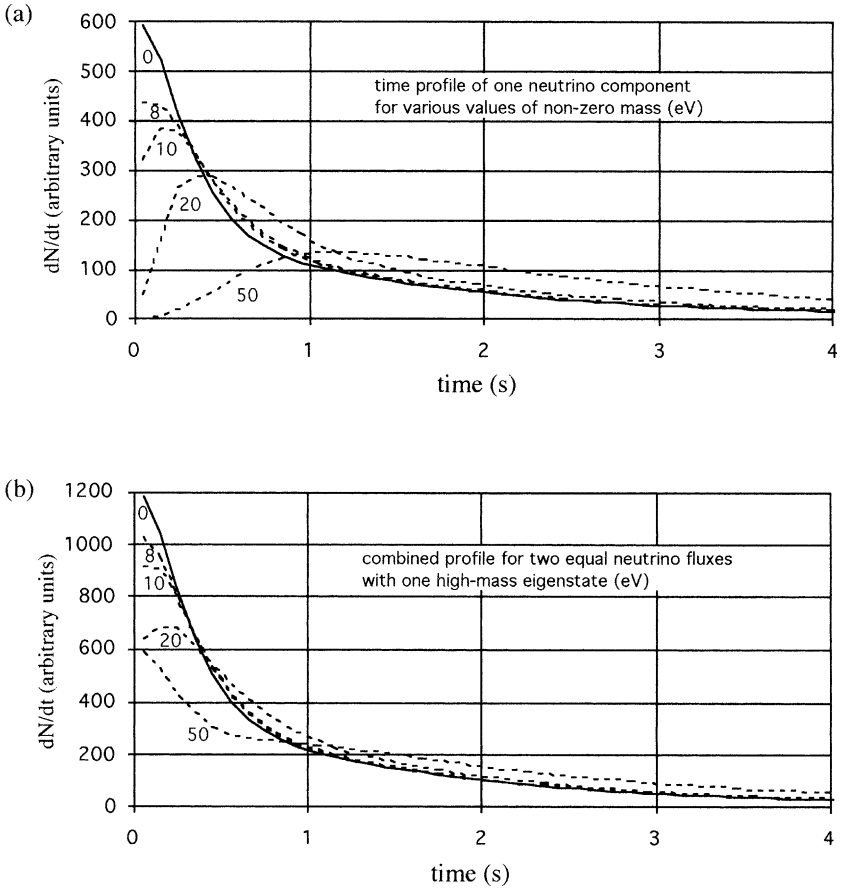

Fig. 3. Typical effects of non-zero mass: (a) effect of non-zero mass on single neutrino component; (b) combination of (a) with equal 'zero mass' component.

estimated within a factor 2 (90% confidence) from a signal of 1000–2000 events.

(e) Fig. 3 suggests that changes in the profile below 1 s could detect masses down to about 8 eV. For 5 eV and below, the profile is essentially coincident with the zero mass profile. Detection of an 8–10 eV mass would be dependent on an accurate knowledge of the zero-mass time profile. If it can be assumed that the time profiles of the different flavours are similar beyond about 0.1 s (as in Fig. 1) then the ~8000 event $\bar{\nu}_e$ time profile from SuperKamiokande [2] would provide a good approximation to the unmodified zero mass shape.

(f) In the case of black hole formation (possibly >25% of cases) mass sensitivity down to a few eV might be achieved from the sharpness of the cut-off in the time profile [46].

(g) If terrestrial neutrino mixing experiments conclude that all neutrino masses lie below 5 eV, then the arrival signals still provide information on neutrino mixing and supernova models. Neutrino mixing signals are discussed further below.

Although the lowest mass detectable by time-of-flight is very dependent on the number of events, one undoubted conclusion is that a ν_τ mass of 20–40 eV – the value which could in principle cluster in the Galaxy and account for all or part of the known dark matter density [23,24] – could be definitively measured or excluded by OMNIS, thus

resolving this long-standing question independently of neutrino mixing scenarios which appear to disfavour this hypothesis.

2.3. Neutrino temperatures and fluxes

It is universally accepted that there will be approximate equipartition of energy between the three neutrino flavours and their antiparticles, and that the typical total energy of the neutrino burst will be $\approx 3 \times 10^{53}$ ergs [16]. The numbers of neutrinos of different flavours will not be quite equal, since the electron neutrinos and antineutrinos decouple at a low temperature than the higher flavours due to the additional interactions $\nu_e + n$, $\nu_e + e^+$, and $\bar{\nu}_e + p$. Typically [16,17] one expects mean energies in the range 10–12 MeV for $\bar{\nu}_e$, 14–17 MeV for ν_e, and 24–27 MeV for $\bar{\nu}_{\mu,\tau}$ and $\bar{\nu}_{\mu,\tau}$. This is consistent with the values 11, 16, 25 MeV, adopted in a number of studies [25–27]. The estimated most probable energy and temperature for supernova 1987a is also consistent with the above assumptions [22].

From these figures we can arrive at 'standard' neutrino fluxes, for purposes of detector calculations, from a supernova at a given distance. We assume a typical value of 8 kpc for the latter, the mean stellar distance being similar to the distance to the Galactic centre. The resulting values for mean energy and integrated neutrino flux are shown in Table 1.

2.4. Effect of systematic uncertainties in supernova strength and distance

Most of the supernovae not in the local 4–5 kpc (~6–7%) of the Galaxy will not be optically visible, though they may subsequently be located by infrared or radio measurements. Thus, initially at least, the parameters subject to some uncertainty will be D (distance kpc), S (total neutrino source strength, ergs), T (neutrino Fermi–Dirac temperature MeV = $1/3 \times$ mean energy, see Table 1).

The total emitted neutrino energy S is believed to be known quite accurately since it is governed not by the initial stellar mass (8–60 M_{sun} [18]) but by the binding energy of the final neutron star, for which $M \sim 1.4 M_{sun}$ and radius $R \sim 10$ kpc [16, 19], giving $S \sim 3 \times 10^{53}$ ergs with an uncertainty $\sim \pm 50\%$ [20]. A typical fit [22] to the events seen from supernova 1987a (at 50 kpc) gave $S = 3 \pm 0.5 \times 10^{53}$ ergs, and $T = 4.5 \pm 0.5$ MeV, in remarkable agreement with the above predictions $S \sim 3 \times 10^{53}$ ergs and $T(\bar{\nu}_e) \sim 5$ MeV.

We can estimate the precision of a mass determination by the following steps:

(i) From Eq. (1) the time profile shape will yield a value or limit on a composite parameter Q related to m_ν, D, T, by

$$Q = D(m_\nu/3T)^2 \tag{2}$$

where m_ν is the mass, $3T$ the mean energy of the neutrino, and D is the distance.

(ii) The distance can be estimated from the assumed source emission $S/6$ for electron antineutrinos, and the neutrino integrated flux F (calculated from the number of charged current events in a water or scintillator detector). The quantities F, S, D are then related by

$$F = (S/6)/(4\pi D^2) \tag{3}$$

(iii) Then since Q and F are the measured quantities, we have, from Eqs. (2) and (3)

$$m_\nu = CT/(S^{0.25}) \tag{4}$$

where C is obtained from measured quantities. The electron antineutrino temperature, believed to be known to $\pm 25\%$, can be independently confirmed from the energy of the observed in-

Table 1
Mean energy and time-integrated flux for different neutrino flavours from a supernova at 8 kpc distance from earth

	ν_e	$\bar{\nu}_e$	ν_μ	$\bar{\nu}_\mu$	ν_τ	$\bar{\nu}_\tau$
Total energy (ergs)	5×10^{52}	5×10^{52}	5×10^{52}	5×10^{52}	5×10^{52}	5×10^{52}
Mean energy (MeV)	11	16	25	25	25	25
Integrated ν flux (ν cm^{-2} at 8 kpc)	3.7×10^{11}	2.5×10^{11}	1.6×10^{11}	1.6×10^{11}	1.6×10^{11}	1.6×10^{11}

teractions in water or scintillator detectors. Thus the remaining uncertainty in mass m_ν is the uncertainty in the quantity $S^{0.25}$.
(iv) As discussed above, S is believed to be constant within $\pm 50\%$ of the standard expectation (5×10^{52} ergs for each of the 6 neutrino types) and the number of events seen from supernova 1987a was consistent with this. Thus the uncertainty in m_ν (or its limit) resulting from the uncertainties in D, S, T, is no more than $\sim(1 \pm 0.5)^{0.25}$ i.e. within $\pm 14\%$.

We can conclude that the uncertainty will be mainly statistical, via the number of events available to fit or limit the time profile distortion parameter Q. The above discussion shows that the distance uncertainty does not result in a major additional error even when the supernova is not seen. If subsequently located by infra-red and radio observations, the latter will provide confirmation of the distance estimated by the above procedure.

3. Neutron production

Neutrinos produce nuclear excitation in the target nuclei, which promptly decay releasing gammas, alphas, protons and neutrons. We are concerned specifically with the neutrons. Wooseley et al. [1] tabulated estimates of total inelastic cross-section, together with branching ratio to neutrons, for a selection of lighter elements up to $A = 34$. We are interested in the use of low-cost target materials. The results tabulated in Ref. [1] enable estimates to be made of neutron production from typical rock targets, and for an iron target. Subsequently Fuller et al. [27] made detailed calculations for salt (NaCl) and for lead, the latter superseding the estimates for lead by Hargrove et al. [28] for the proposed LAND supernova detector. Fuller et al. also include estimates for both single and double neutron production (discussed in more detail later in this paper). More recently Kolbe and Langanke [29,30] have made independent estimates of the neutron production from Fe and Pb.

The results of these three sets of estimates are summarised in Table 2, expressed as neutrons produced per ton of target for a supernova at 8 kpc, using the integrated fluxes in Table 1. The results are shown for each neutrino type, with contributions from both neutral and charged current excitation in the case of ν_e and $\bar{\nu}_e$ ([27,29,30].

The table shows a large measure of agreement in both the trend with atomic mass and the absolute values. Estimates [1] and [27] agree in the general magnitude of production from the lighter minerals – about 0.02–0.03 ton^{-1}. Estimates [1] and [29,30] agree that neutron production will be higher in Fe – about 0.1–0.2 ton^{-1}, the majority of the increase coming from the higher branching fraction to neutrons. We assume the value 0.2 ton^{-1} on the basis of the more detailed study in [29,30]. With lead, the production is agreed by [27] and [29,30] to be higher still, with the factor $\sim$2 difference between the two estimates being ascribed in Refs. [29,30] to an additional contribution from forbidden transitions in [27]. We therefore provisionally assume the higher figure.

On this basis, the final column of Table 2 represents the current best estimate of neutron production from the targets NaCl, Fe, and Pb, for which we will assume the values of 0.03, 0.2, 0.9 events per ton for an 8 kpc supernova. In each case, the neutron production is dominated by the contribution from the higher neutrino flavours, so that in this respect OMNIS would complement existing world detectors, SuperKamiokande, SNO, LVD, based on large-volume water and scintillator targets (see Table 1 in Ref. [2]) and the new KamLAND project [42].

4. Neutron collection

Neutrons are expected to be produced with a typical nuclear evaporation spectrum of the form

$$dN/dE = C(E/E_0)^\alpha \exp(-E/E_0) \quad (5)$$

where $\alpha < \sim 0.5$, C is a normalising constant, and E_0 is a characteristic energy in the region 1.2–1.5 MeV.

This is confirmed by the calculations of Kolbe and Langanke [29,30] who calculate typical spectra, from both neutral and charged current

Table 2
Estimates[a] of number of neutrons produced per ton of target material for supernova at 8 kpc, from calculations of Wooseley et al. [1], Fuller et al. [27] and Kolbe and Langanke [29,30]

Reference	Target	Neutral or charged current	ν_e	$\bar{\nu}_e$	$\nu_{\mu,\tau} + \bar{\nu}_{\mu,\tau}$	Totals	Total neutrons/ton (n + c)
[1]	SiO_2	nc	0.0001	0.001	0.020	0.021	
[1]	$CaCO_3$	nc	0.0005	0.001	0.016	0.017	
[1]	'NaCl' [b]	nc	0.0000	0.002	0.022	0.024	
[27]	NaCl	nc	0.0001	0.001	0.021	0.022	
		cc	0.0000	0.005	–	0.005	
							0.03
[1]	Fe	nc	0.0022	0.013	0.089	0.104	
[29,30]	Fe	nc	0.0000	0.012	0.178	0.190	
		cc	0.0000	0.009	–	0.009	
							0.20
[29,30]	Pb [1n]	nc	0.0048	0.003	0.304	0.312	
		cc	0.1110	0.001	–	0.112	
[27]	Pb (1n)	nc	0.0080	0.039	0.702	0.749	
		cc	0.0520	0.000	–	0.052	
[27]	Pb (2n)	nc	0.0002	0.002	0.041	0.043	
		cc	0.0540	0.000	–	0.054	
							0.90

[a] 3–4 decimal places are used in this table for comparison between small and large contributions, but model approximations contain uncertainties of typically ±30–50% [27] and only the first non-zero digit is significant.

[b] Na and Cl are not among the nuclei tabulated in [1] but were estimated using results for neighbouring elements. The result is similar to that in [27] using Na and Cl.

excitation, which can be approximately fitted by parameters in the above range. If the target material has sufficiently low neutron absorption, the majority of these neutrons will escape from the target after typically 200–1000 scatters and can then be thermalised and absorbed in external detectors such as slabs of Gd- or Li-loaded scintillator. This process takes typically less than a millisecond, so does not significantly affect measurement of the neutrino time profile.

It was shown in the previous paper [2] that transmission of the signal to detector by neutron multiple scattering allows, in principle, a considerable range of choices of target and detector geometry, and the neutron collection also has a substantial dependence on target material. Monte Carlo results for a range of minerals and metals showed more than an order of magnitude improvement in the collection of neutrons in progressing from light minerals (salt, chalk) to a heavy metal (lead). This is in addition to the gains in neutron production summarised in Section 3 above, so that there is potentially a combined gain of up to two orders of magnitude in neutron signal from a lead target compared with a rock target.

To compare specific figures for the targets NaCl, Fe, Pb, comparative Monte Carlo simulations have been made for the test case of a single slab of 0.5% Gd-loaded hydrocarbon scintillator, dimensions 6 m × 2 m × 0.2 m, in the centre of a cavern 6 m × 6 m × 12 m lined with a 1 m thickness of each material (Fig. 4). The results are summarised in Table 3, both for a constant neutron production of 0.1 ton^{-1} of target and then adjusted for the material-dependent production in the final column of Table 2. It should be noted that low cost silica-based materials, such as sand and concrete, give a similar neutron production and about 25% greater neutron capture efficiency, and improve only slightly on NaCl, typically from 0.08 to 0.1 neutrons m^{-2}.

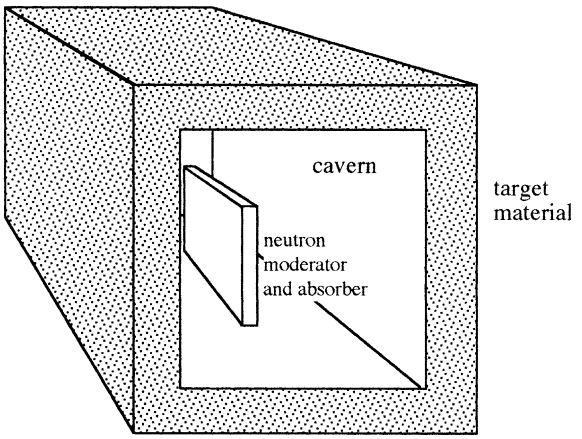

Fig. 4. Test geometry for comparative simulations of transport of individual neutrons from different target materials to moderation and absorption in scintillator slab.

It is evident that the substantial gain in neutron signal available from lead and iron targets produces a large reduction in detector area needed. The test geometry, of Fig. 4 however, while reasonable for an existing rock cavern, would require an unrealistically large amount of material in the case of artificial targets, unless these happen to be available at negligible cost (e.g. as surplus shielding from previous uses). More usually, a different geometry must be used to minimise the total cost of target + detector, as discussed below. At the same time, the absolute neutron collection efficiency becomes important to optimise the two-neutron signal resulting from neutrino mixing. This will be discussed in Sections 5 and 6.

5. Neutrino mixing

Oscillations between ν_μ and ν_τ are not observable from the supernova burst because it contains equal numbers of each, with no difference in the (neutral current) interaction with the target. In contrast, oscillations between $\nu_{\mu,\tau}$ and ν_e can produce an observable effect through the production of higher-momentum ν_e, giving an increase in neutron production through the increased charged current excitation cross-section.

This has been studied by Fuller et al. [27] who calculate the expected increase in neutron production and in addition find an even larger increase in the cross-section for two-neutron production. Specifically, if there is an MSW transition from ν_τ or ν_μ to ν_e in the high density of the supernova (up to 10^{10} g cm^{-3}) this reduces the flux of the higher flavours by 25% but converts this fraction into a ν_e flux of mean energy 25 MeV, for which there is an increased charged current cross-section for both 1n and 2n production. Using the cross-sections and branching ratios tabulated in Ref. [27] the events per ton with and without mixing are shown in Table 4 (these figures are calculated for an MSW transition of one flavour – either ν_μ or ν_τ to ν_e but not both).

Table 3
Monte Carlo estimates[a] of neutron absorption for different target materials in test configuration of Fig. 4. Final column shows effect of multiplying by the theoretical production factors in Table 2

Target material	Neutrons absorbed in 12 m^2 detector (%)	Neutrons captured per m^2 detector for production 0.1 ton^{-1}	Estimated neutron production per ton from Table 2	Neutrons captured per m^2 detector for 8 kpc supernova
NaCl	6.9 ± 0.4	0.34 ± 0.02	0.024	0.08 ± 0.01
Fe	6.3 ± 0.4	1.12 ± 0.08	0.20	2.2 ± 0.2
Pb	17.0 ± 0.6	4.36 ± 0.16	0.90	39 ± 2

[a] As a check on the author's Monte Carlo tracking program used in this and the preceding paper, simulations for this table were repeated by McMillan (University of Sheffield) using the established 'MCNP' programme. The results for each material agreed with column 2 within the stated errors. Since this test geometry includes all key processes – scattering in target, long range cavern scattering, thermalisation and absorption in the detector, the agreement constitutes an adequate check that the two programs do not differ significantly for neutron transport, at least for energies up to 10 MeV.

Table 4
Estimates of number of neutrons produced per ton of lead target with or without conversion of ν_μ or ν_τ to ν_e for supernova at 8 kpc, from Ref. [27]. In this table the 2n figures refer to 'events per ton' (i.e. neutron pairs per ton) the number of neutrons being twice this as listed in Table 2

Target, 1n or 2n	ν_μ or ν_τ conversion to ν_e	Neutral or charged current	ν_e	$\bar{\nu}_e$	$\nu_{\mu,\tau} + \bar{\nu}_{\mu,\tau}$	Totals	Total events per ton (n + c)
Pb, 1n	None	nc	0.008	0.039	0.702	0.749	
		cc	0.052	0.000	–	0.052	
							0.80
Pb, 1n	Full	nc	0.182	0.039	0.521	0.742	
		cc	0.911	0.000	–	0.911	
							1.65
Pb, 2n	None	nc	0.0001	0.001	0.021	0.022	
		cc	0.027	0.000	–	0.027	
							0.05
Pb, 2n	Full	nc	0.005	0.001	0.015	0.022	
		cc	1.87	0.000	–	1.87	
							1.89
Fe, 1n	None	nc	0.000	0.012	0.178	0.190	
		cc	0.000	0.009	–	0.009	
							0.20
Fe, 1n	Full	nc	0.045	0.012	0.134	0.191	
		cc	0.072	0.009	–	0.081	
							0.27

The key conclusion, discussed in Ref. [27], is that while the single neutron rate will be increased by mixing, this may be masked in practice by uncertainties in the absolute cross-sections, whereas the ratio of 2n to 1n events is less affected by absolute cross-section uncertainties and shows a clear factor ~40 increase in the presence of mixing. Production of neutron pairs will not be significant in lighter elements, so Fe would provide an important comparison target, confirming any mass distortions of the time profile in Pb, but not showing the two-neutron mixing signal. Thus the use of two target elements is an important feature of the proposed OMNIS detector.

To illustrate the sensitivity of OMNIS to neutrino mixing, the coverage of the 'MSW triangle' on the standard Δm^2 versus $\sin^2 2\theta$ plot is much larger than for solar and terrestrial experiments because of the wide density range (10^{10}–10^{-4} g cm^{-3}) in the supernova envelope. If no mixing is observed, the apex of the excluded region extends to 10^{-10} in $\sin^2 2\theta$ and from $\Delta m^2 = 10^4$–10^{-10} eV^2 [16,45]. In addition, because of the long flight path, vacuum mixing would be observable down to $\Delta m^2 \sim 10^{-19}$ eV^2.

6. Optimisation of one- and two-neutron collection efficiency

The need for both the single and double neutron time profile introduces the need use a design which maximises both the total number of events and the collection efficiency from the target. Since the two neutrons in a two-neutron event are emitted in random directions, such an event would be detected by defining a short time window within which the two neutrons are coincident. Thus if OMNIS is subdivided into a number of independent detector modules, the relative efficiency for the collection of two-neutron events is equal to the efficiency η for observation of single neutrons from the target mass in a given module.

In assessing possible geometric arrangements, there arises the need to compromise between absolute efficiency and cost. The arrangement of

Fig. 4, which minimises the detector area needed to collect a given number of events, has also a low value for η (17% from Table 3). At the other extreme, one may cover the surface of small volumes of target with detector to achieve, in principle, neutron collection efficiencies exceeding 90% but this reduces the events collected per unit detector area from the value 30–40 m^{-2} in Table 3 to <2 m^2 – e.g. in the case of 1–1.5 m cube of lead surrounded by scintillator slabs. This represents the useful upper limit in linear dimension for individual target blocks, since larger non-subdivided targets will exceed the escape distance (projected range $\sim$0.7 m) for neutrons in lead.

A series of configurations linking these two extremes is shown in Fig. 5, together with a plot

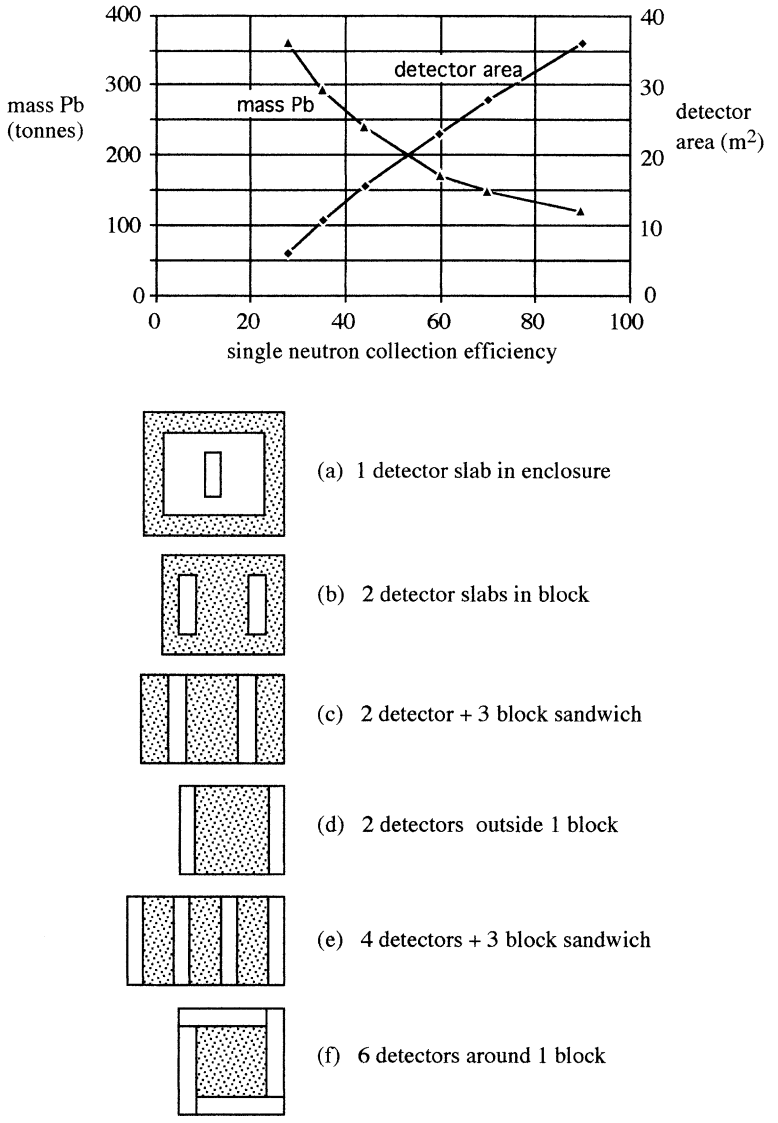

Fig. 5. Examples of detector–target configurations of progressively greater neutron collection efficiency, with corresponding target masses for fixed total number of events ($\sim$100 events for supernova at 8 kpc). The plotted points correspond, from left to right, to the six sketched configurations (a)–(f).

summarising the results of Monte Carlo simulations relating target mass, neutron collection efficiency, neutron collection efficiency, and detector area. The individual dimensions were adjusted to achieve the same neutron collection (i.e. number absorbed in detector) in each case. Other arrangements are possible, such as a larger number of individual circular or square cross-section detectors distributed throughout the lead target, as proposed for the LAND project [28]. Note that the collection efficiency in Fig. 5 is governed principally by detector area rather than detector mass, since the detector thickness is in general fixed by the neutron detection technique. In the case of, e.g., Gd-loaded scintillator about 3–5 cm thickness is required to thermalise and absorb the neutrons and an additional 20–30 cm thickness to convert the emitted gammas. Further increase in thickness does not significantly increase the number of neutrons detected. Other neutron detection methods are discussed in Section 7.

To illustrate the typical design and performance choices, we consider in more detail the two 'sandwich' arrangements (c) and (e) of Fig. 5, either of which would be suitable for the construction of individual OMNIS modules in a large array. As useful prototype module would be one achieving 100 events for a supernova at 8 kpc, and this could then be replicated into a larger array. Fig. 6 shows a set of dimensions for module types 5c and 5e which would achieve 100 events absorbed in the loaded scintillator slabs. Table 5 summarises the collection efficiency and events collected for each of these. The numbers take account of the fact that for some of the two-neutron events only one neutron will be seen. For a production of N_1 single neutrons and N_2 double neutrons, and for a single neutron collection efficiency η, the observed numbers of 1 and 2 neutron events will be

$$N_1\ (\text{obs}) = N_1\eta + 2N_2\eta(1-\eta) \tag{6}$$

$$N_2\ (\text{obs}) = N_2\eta^2 \tag{7}$$

from which it is also apparent that using Monte Carlo estimates of η, one could obtain the true values N_1, N_2, from the observed values N_1 (obs), N_2 (obs).

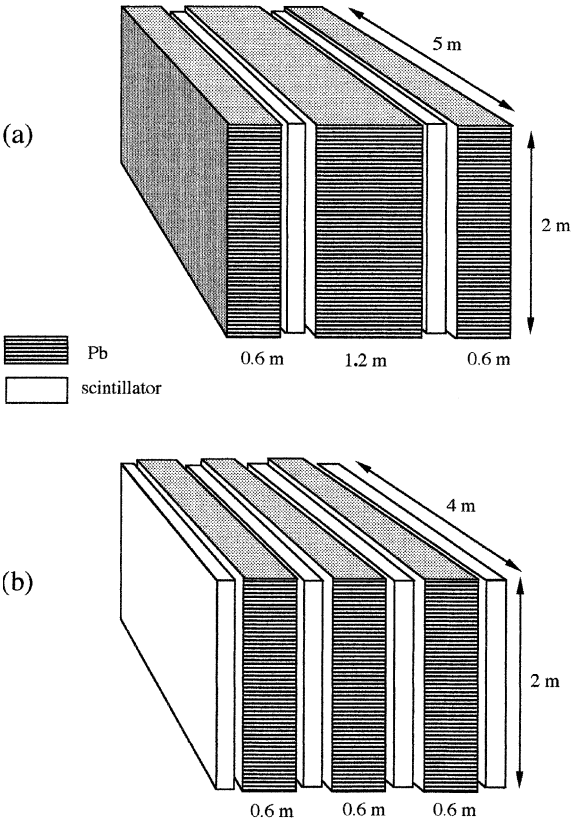

Fig. 6. Examples of designs collecting 100 events from a supernova at 8 kpc: (a) moderate collection efficiency, corresponding to Fig. 5(c); (b) high collection efficiency, corresponding to Fig. 5(e).

It can be seen from the numbers in Table 5 that, for a fixed number of events the observed ratio of double to single neutron events changes from ~2% to ~22% for full MSW mixing in the case of a Fig. 6a configuration and from ~4% to ~50% in the case of a Fig. 6b configuration. This example shows that a design of lower absolute efficiency can achieve a satisfactory mixing signature at a lower cost/event than a higher efficiency design requiring more detector area (the latter being in general the dominant cost component). Fig. 7 shows the number of single and double neutron events versus collection efficiency for the example of a Pb target mass 250 tons, with or without MSW conversion, using Eqs. (6) and (7) and the neutron production figures from Table 4.

Table 5
Comparison of two '100-event' systems with different neutron collection efficiencies, showing estimated numbers of single and double neutron events with and without MSW mixing in supernova

Design type	Pb mass (tons)	Scintillator total area (m^2)	Neutron collection efficiency, η	No mixing		Full MSW conversion ν_τ or $\nu_\mu \rightarrow \nu_e$	
				1n	2n	1n	2n
Fig. 6a	260	20	0.44	98	2	430	95
Fig. 6b	160	32	0.73	96	4	310	155

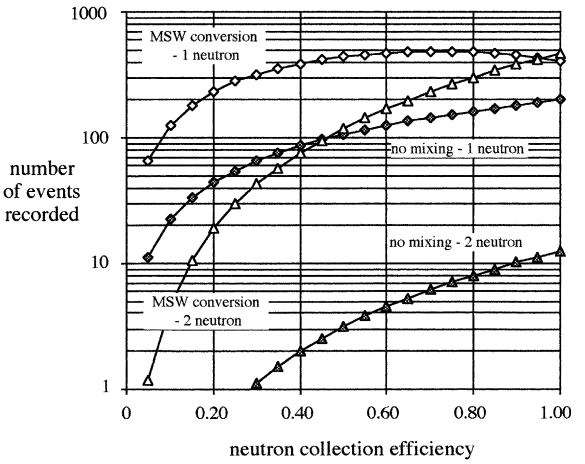

Fig. 7. Effect of collection efficiency on recorded number of single and double neutron events, with and without mixing, for 250 ton Pb target and supernova at 8 kpc.

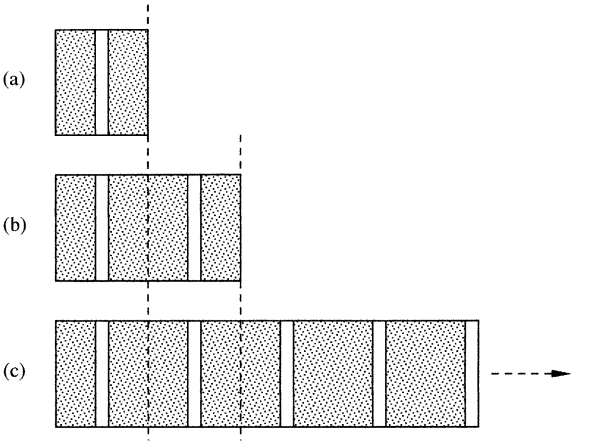

Fig. 8. Improvement in collection efficiency η in alternating detector/target arrays: (a) $1/D = 1$, $\eta = \eta(1)$; (b) $1/D = 0.5$, $\eta(2) = 1.5\eta(1)$; (c) $1/D \ll 1$, $\eta(\infty) \rightarrow 2\eta(1)$.

The optimum proportions for design 5c occur when the outer blocks are approximately half the width of the inner, with the latter in the range 1.2 ± 0.2 m. For larger systems, modules can be placed together to form a continuous alternating sandwich structure of higher efficiency. For an assembly of D detector slabs interleaved between $D+1$ target blocks, simple symmetry considerations (i.e. that neutrons random walk equally to left and right) indicate that the collection efficiency η will vary in proportion to $(1 - 1/2D)$. Thus a single detecting plane sandwiched between two target slabs (Fig. 8a) would have about $1/2$ the neutron collection efficiency compared with a continuous array (Fig. 8c), and for the case of two detecting planes between three target slabs (Fig. 8b) the reduction would be about $3/4$. Thus for a typical continuous array, illustrated in Fig. 9, one would expect to improve the collection efficiency η to a value in the range 50–60%. However, for an OMNIS system built up over a period of time, it is perhaps more likely that a series of independent modules would be constructed along an underground tunnel, and would be sufficiently separated (e.g. 2–3 m) for the neutron collection efficiencies to remain at the single module value.

In the case of two-neutron events, each of the neutrons will be emitted isotropically and may register in the same or different detector slabs. Thus a two-neutron event is identified by a coincidence window chosen to collect the majority of such events while minimising false two-neutron events due to coincidence between single neutrons. Fig. 10 shows the integral distribution of neutron capture times obtained by Monte Carlo simulation of the geometry of Fig. 6a, the time distribution being also similar for the case of Fig. 6b. This shows that >95% of the neutrons are captured

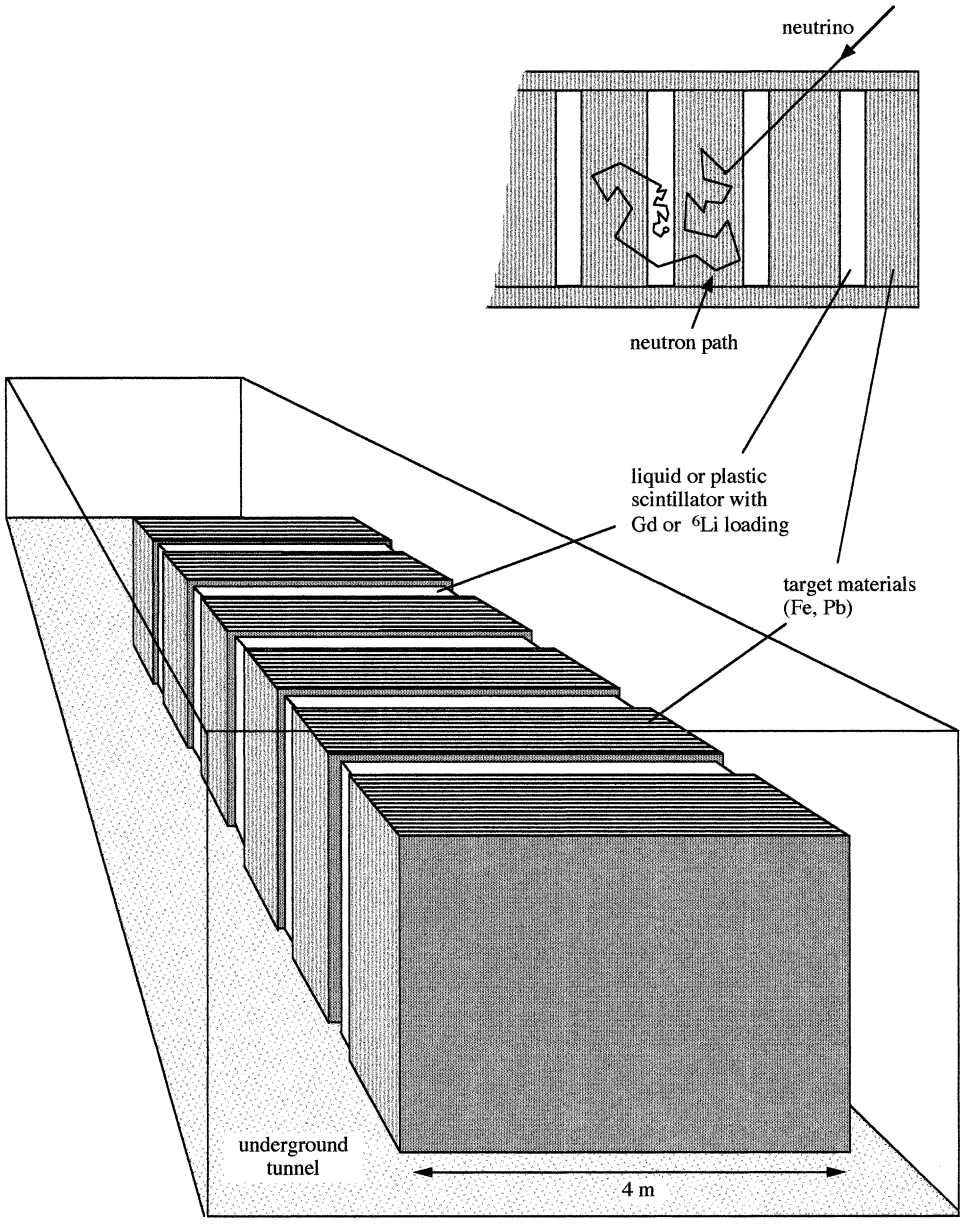

Fig. 9. Portion of typical OMNIS array using continuous sandwich geometry for maximum collection efficiency (schematic only – shielding around detector edges not shown). Inset shows typical neutron path following neutrino excitation of target nucleus.

within 0.1 ms and >99% are captured within 1 ms. Taking 0.1 ms as the coincidence window (and assuming 70% of the neutrinos arrive in the first 2 s) the false coincidences in a 100-event module are

1. For no mixing, mean single neutron rate 50 s^{-1}, false coincidences ~0.5.
2. With full MSW conversion, mean single neutron rate 200 s^{-1}, false coincidences ~8.

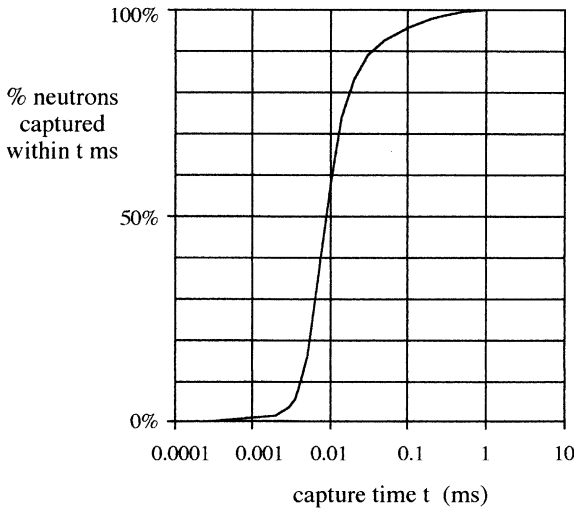

Fig. 10. Integral distribution of neutron capture times for geometry of Fig. 6a.

Thus with a 0.1 ms coincidence window the false coincidences alter the two neutron rate from ~2% to ~2.5% in the no-mixing case, and from ~22% to ~24% with full MSW conversion. This shows that the 'sandwich' designs of Fig. 6 provide sufficiently fast neutron collection times to allow the fraction of two neutron events to be measured with sufficient accuracy. In practice the arrival time of all neutron pulses would be recorded, and an optimum coincidence window selected and applied in the analysis stage.

7. Neutron detection and identification

The preceding results are obtained from simulations of neutron absorption in a combined moderator and absorber, e.g. Gd or Li-loaded hydrocarbon, the object being to investigate the number of neutrons collected and absorbed as a function of target and detector geometry. The absorption events must then be converted to a signal, and distinguished from background. This will in general be achieved with less than 100% efficiency, so that it is important to ensure that detection methods are chosen which minimise loss of events in the conversion and identification process.

Taking the example of Gd-loaded liquid scintillator, neutrons emerging from the target with a range of energies will all be thermalised in about 3 cm of hydrogenous material. They will then be absorbed by either an H or Gd nucleus, releasing MeV-range gammas. The aim is for the majority to be absorbed on the Gd, giving the distinctive signal of typically 4 gammas totalling 8 MeV in energy. With 0.5% Gd by weight, uniformly distributed in the scintillator, $94 \pm 1\%$ of the neutrons are absorbed on the Gd, the remainder being absorbed on the H (also giving gammas but totalling 2.2 MeV). It then requires a thickness ~25 cm scintillator to convert sufficient of the gamma energy by Compton scattering, to distinguish the event unambiguously from gamma background (which extends to ~2.6 MeV from Th). About half the gamma energy is lost from the scintillator boundaries, still leaving an average of 3–5 MeV deposited by the neutron absorption events.

This situation is illustrated schematically in Fig. 11, showing the overlap between the typical gamma spectrum from neutron absorption events in the loaded scintillator and a typical background gamma spectrum <2500 keV resulting from U/Th contamination in nearby materials and components [47,48]. Thus the neutron discrimination can be improved by reducing gamma background, in particular by the use of low background target materials and a water or oil buffer to shield the scintillator from the photomultipliers [32]. Since only 3 cm of scintillator is required to moderate the neutrons, the substantial extra thickness required for the Compton gamma conversion is a disadvantage of the use of Gd. This additional thickness is not required in the case of loading with ^{6}Li or ^{10}B in which neutron absorption produces micron-range recoiling nuclei. However, this saving in detector volume is accompanied by the disadvantage that the MeV energy deposit is in both cases quenched to an electron-equivalent energy of only a few hundred keV, thus dropping all of the signal into the gamma background.

The mean gamma background in Fig. 11 is largely time independent and can therefore be subtracted leaving positive or negative Poisson errors in each time bin. Thus neutron events can still be counted in the overlap region, but with a

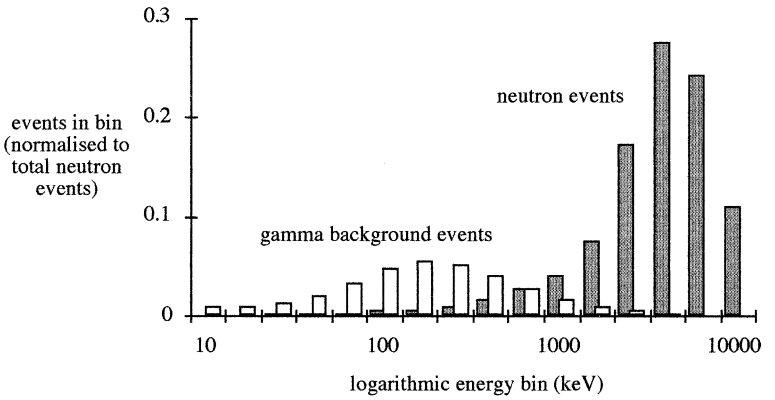

Fig. 11. Typical overlap between Gd-gamma signal and gamma background.

reduced accuracy dependent on the relative magnitudes of neutron and gamma events in each time interval. Thus the gamma background affects mainly the observation of the tail of the supernova burst.

The use of loaded scintillators has the basic merit that the moderator, absorber and converter are uniformly mixed, giving the best conditions for high detection efficiency. The loading, however, may not have long-term stability, giving rise to a reduction in transparency over a period of many years [33]. A number of alternatives may be considered, in which only two of the functions are combined, with the other function remaining separate. These variations are summarised in Table 6, in which the loaded scintillator is designated Type 1, with schemes involving separate moderator, absorber or converter designated Types 2, 3, and 4, respectively. The table also gives specific examples of each type with sample references. No examples of Type 4 appear to have been published, though for this project it may prove the best option for achieving adequate efficiency combined with long term stability. Fig. 12 gives typical geometric arrangements and typical dimensions for each type.

Monte Carlo simulations were carried out for Type 1, Type 2, and Type 4, using Gd as absorber in each case, to compare detection performance in terms of overlap with gamma background. Fig. 13a shows the results expressed as the integral number of events (normalised to unity) for increasing recorded energy in the scintillator (up to the maximum of 8 MeV available from the Gd gammas). Greater spread to lower energies increases the overlap with gamma background. It is seen that Type 4 shows a slightly greater spread

Table 6
Classification of neutron detector types according to relative location of moderator, absorber and signal converter

	Type 1	Type 2	Type 3	Type 4
Principles				
Separate component	–	Moderator	Absorber	Converter
Combined components	Moderator, absorber, converter	Absorber, converter	Moderator, converter	Moderator, absorber
Examples				
Separate component		H or C-based moderator	Gd foils or coatings [40]	Pure scintillator
Combined components	Gd, ^{6}Li, or ^{10}B loaded hydrocarbon scintillator [31–36]	Scintillation: ^{6}Li + ZnS [37,38] ^{6}Li + Ce-glass [37,38] ^{6}Li fibres [39]	Pure scintillator	Gd in hydrogenous material
		Gas proportional: BF_3, ^{3}He [31]		

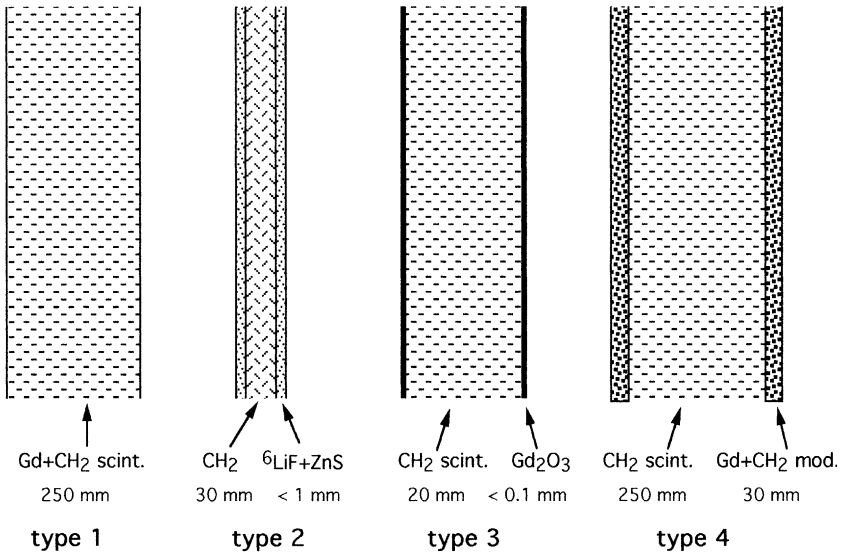

Fig. 12. Principal types of low energy neutron detector, showing different arrangements of moderator and absorber.

than Type 1, due to the loss of gamma energy in the separate moderator, while Type 3 shows a further spread due to over half of the neutrons being absorbed on H instead of Gd. There is also a decrease in absolute number of events registered in the scintillator. The effect of including this is shown in Fig. 13b, in which Types 3 and 4 are shown relative to the number collected by Type 1 instead of separately normalised. This illustrates the fact that Type 3, where the Gd is separate, gives both a substantial absolute reduction in events detected and a greater overlap with any gamma background, whereas these effects are less significant in the case of Type 4 where the Gd remains associated with the moderator. Note that in the latter case, the Gd-hydrocarbon mixture does not need to be either scintillating or transparent, since most of the Gd gammas escape into the adjacent pure scintillator.

These results do not include the additional identifying advantage of Type 1, which can also register the neutron energy deposited directly in the scintillator during the thermalisation process. Observation of both the thermalisation signal and the Gd absorption signal could provide better neutron identification [41].

The various Type 2 (separate moderator) arrangements in Table 6 involve a wider range of materials and cannot be included in the comparison of Fig. 13. The merit of many of these is that they have much reduced gamma sensitivity (due in particular to the low thickness) so that the problem illustrated in Fig. 11 is less important. However, absolute efficiencies are relatively low with these schemes, making them less suitable for OMNIS unless unlimited target material is available. Separate moderator in general achieves no more than 20–30% efficiency in the case of hydrocarbons and 10–15% efficiency in the case of carbon, the latter requiring 15–20 cm thickness to thermalise neutrons compared with 3 cm for hydrocarbons. In addition, all the Type 2 schemes are in general more costly per unit collection area. Nevertheless the property of gamma insensitivity could still make the use of Li–ZnS sheets, for example, an economic choice in conjunction with recycled target material (Fe or Pb) which may have a higher gamma activity than new material.

8. Neutron backgrounds

The magnitude and effect of the continuous underground neutron background was discussed in the previous paper [2]. It was shown that the

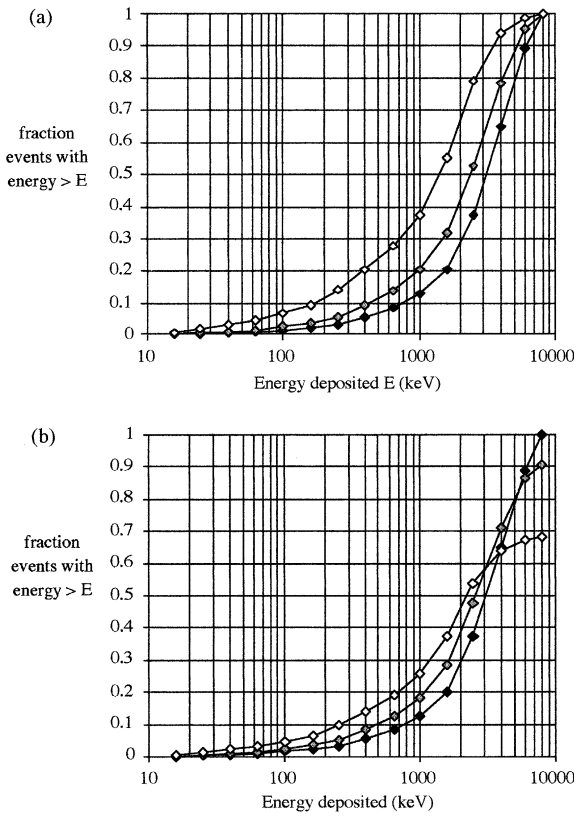

Fig. 13. Integral signal distributions for neutron detector geometries of Fig. 12: Type 1 (solid points), Type 3 (unfilled), Type 4 (shaded): (a) each individually normalised to unity; (b) each normalised to total for Type 1.

backgrounds are small compared with an 8 kpc supernova signal during the first few seconds of the burst, but it is of interest to estimate how well the tail of the time profile can be observed, and at what distance the supernova signal will fall below background. We consider the specific example of the Boulby salt mine (UK) which has a depth of 1100 m. There are three main sources of neutron background:

1. Cosmic ray muons are estimated to produce $\sim 3 \times 10^{-5}$ neutrons ton^{-1} s^{-1} target material at a depth of 1100 m [2].
2. Uranium and Thorium produce neutrons by alpha spallation. Lead contains typically only 0.01 ppb U or Th, producing 10^{-6} neutrons ton^{-1} s^{-1}. An iron target may have U/Th levels 100 times this, depending on the source of the material.
3. The underground rock has U and Th levels $\sim$100 ppb, resulting in a cavern neutron flux $\sim 5 \times 10^{-3}$ neutrons m^{-2} s^{-1}. Monte Carlo simulations show that this external flux penetrates the proposed module with an attenuation factor $\sim$0.1 before reaching the detector. This could, if necessary, be further attenuated with hydrocarbon shielding.

These continuous backgrounds are compared with the signal in the following table, normalised to rates per 100 tons target material:

Time after start of burst:	Production rates per second per 100 tons		
	1 s	4 s	20 s
Neutron production in Pb target (8 kpc)	50	4	1
Neutron production in Pb target (20 kpc)	8	0.6	0.16
Neutrons diffusing from cavern walls	0.01	0.01	0.01
Neutrons from cosmic ray muons	0.003	0.003	0.003
Neutrons from U/Th in target	0.0001	0.0001	0.0001

Thus, even at 20 s after the start of the burst, the neutron backgrounds remain small compared with the signal for both the mean and largest Galactic supernova distances. Moreover, the mean continuous level can be subtracted from each time bin, leaving Poisson fluctuations in neutron background much smaller than the Poisson fluctuations of the signal itself.

9. Possibility of combining with solar neutrino detection – SIREN

Detectors based on Cerenkov detection in a water target, such as SuperKamiokande and SNO, are able to detect both supernova $\bar{\nu}_e$ and solar

ν_e, through charged current interactions with a threshold of a few MeV. OMNIS specialises in detection of higher flavour neutrinos through higher threshold neutral current nuclear excitation, an interaction which does not have a useful sensitivity to solar neutrinos. However it was proposed by Ragahavan [6,7] that real time solar neutrino spectroscopy could be achieved by charged current excitation of Gd or Yb targets which provides, in addition to the prompt electron, a delayed coincident low energy gamma to identify these events from gamma background. In this way, a real time energy spectrum could be achieved in the energy range 0.3–2 MeV for the first time. UK studies of this scheme adopted the acronym SIREN (Solar neutrino Interactions by Real-time Excitation of Nuclei).

An intriguing feature of this proposed technique is that it requires Gd-loaded scintillator within lead shielding, thus suggesting the possibility of a detector which would use Gd as a target for SIREN while simultaneously acting as neutron absorber for OMNIS, each using the same scintillator to register signals [8,9]. The Pb could be configured to act as shielding for SIREN while providing the target for OMNIS (Fig. 14).

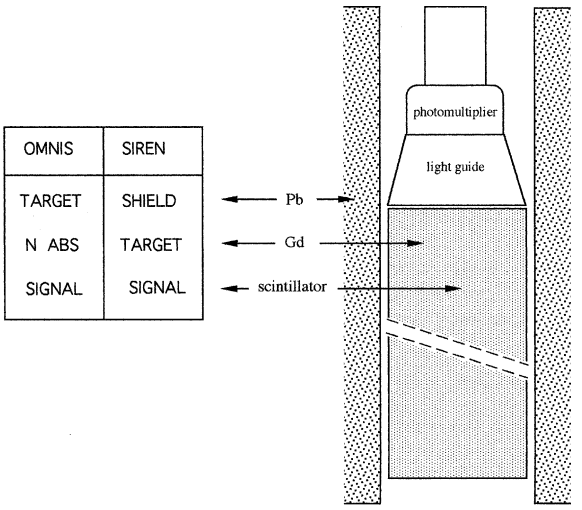

Fig. 14. Principle of combined OMNIS and SIREN solar neutrino detector, doubling the functions of the principal component materials.

Although using similar materials, there are several key differences in the requirements of OMNIS and SIREN:

1. The Gd/scintillator ratio (by weight) needs to be only 0.2–0.5% for OMNIS but 5–10% for SIREN (to obtain sufficient target mass [6,7]).
2. The scintillator energy threshold can be >1 MeV for OMNIS, but needs to be $<\sim$70 keV for SIREN, to observe the coincident gammas from nuclear de-excitation.
3. There are low energy background events which can mimic a SIREN signal, and which must thus be reduced to below signal level.

The principal example of 3 is the alpha decays from ^{152}Gd. Although these have energy 2 MeV, the alpha signal is quenched to 200–300 keV in liquid scintillator and might mimic the tagging signal in delayed coincidence with a higher energy gamma, the latter then being mistaken for a converted electron from an incident neutrino. We assume a fraction f of alphas simulate a gamma $\sim$60 keV by partial energy deposition near a boundary. For a given individual module size, the rate of such coincidences can then be estimated as follows:

- decay constant of $^{152}\mathrm{Gd} = 5.0 \times 10^{21}$ s
- fraction ^{152}Gd in natural Gd $= 0.002$
- alpha rate in M (kg) natural Gd $= 1.32 \times 10^5\ M\,\mathrm{d}^{-1}$
- alpha rate simulating tag in M (kg) natural Gd $= 1.32 \times 10^5\ fM\,\mathrm{d}^{-1}$
- assumed background gamma rate in range 0.1–1 MeV $= B\ \mathrm{kg}^{-1}\,\mathrm{d}^{-1}$
- assumed coincidence time window $= w$ ns
- alpha/gamma coincidence rate $= 1.52 \times 10^{-9}\ fwBM^2\,\mathrm{d}^{-1}$
- estimated signal rate in 10000 kg natural Gd [6,7] $= 0.55\ \mathrm{d}^{-1}$
- corresponding signal rate in sub-volume of mass M (kg) $= 5.5 \times 10^{-5}\ M\,\mathrm{d}^{-1}$
- Hence: ratio r of simulated events to real events $= 2.8 \times 10^{-5}\ fwBM$

Thus for typical values $B = 200\ \mathrm{kg}^{-1}\,\mathrm{d}^{-1}$, $f = 0.001$, $w = 100$ ns, we obtain $r = 5 \times 10^{-4}\ M$ (kg), indicating that the simulated events can be reduced

to <1% of the signal events by subdivision of the 10 ton target into sub-units containing <10 kg Gd. For 5–10% Gd loading, this means individual scintillator cells of volume ~0.1–0.2 m^3, for example with dimensions 0.2 m × 0.2 m × 3 m. If the required energy resolution can be achieved in detection cells of this type, they could then be assembled in arrays interleaved with, or surrounded by, lead shielding, and would then also have a high efficiency for detection of an OMNIS signal from the lead. Schematic examples are shown in Fig. 15. It has been suggested that spurious simulated events involving partial alpha energy deposits might be eliminated by using wavelength-shifting plastic scintillator to contain the Gd-loaded liquid scintillator [43].

The provisional conclusion is that a combination of OMNIS and SIREN would be possible in the sense that a high resolution low threshold SIREN array can be designed to provide also an OMNIS signal, but for OMNIS alone the detector modules can be designed more simply at lower cost. The most attractive combination might thus be an array of minimum cost OMNIS modules together with a separate array of SIREN modules which would also provide an OMNIS signal. Some modules would be built with iron shielding to provide a comparison target giving a single neu-

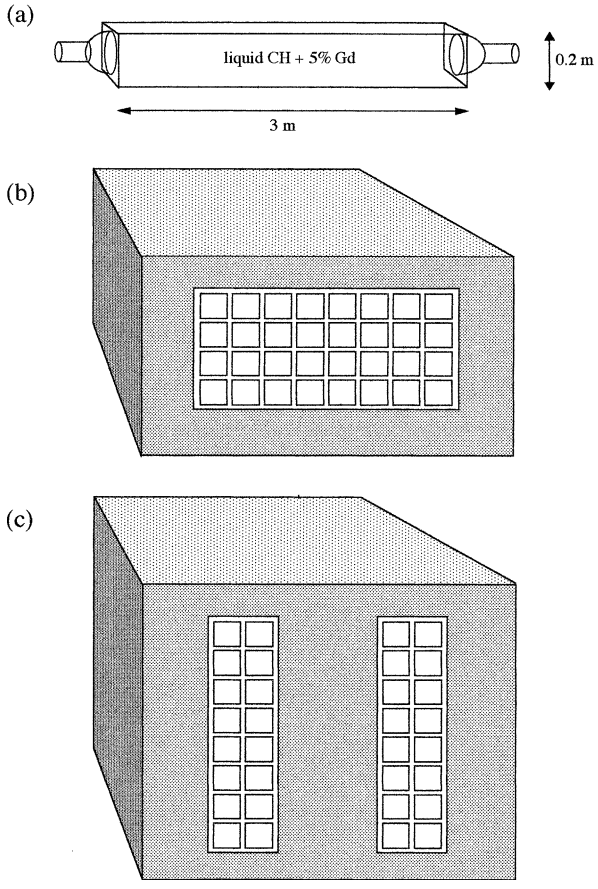

Fig. 15. Possible OMNIS/SIREN configurations: (a) typical SIREN sub-unit (0.1–0.2 m^3); (b) SIREN array with surrounding OMNIS target; (c) SIREN array doubling as OMNIS design of Fig. 6a.

tron time profile but without a two-neutron mixing signal (Table 4).

10. Conclusions

The rarity of Galactic supernovae, combined with the wealth of particle physics and astrophysics information which can be obtained by observing the neutrino burst, leads to the need for a full range of world detectors running continuously to record the time profile of all three neutrino flavours. Existing and planned detectors based on water and liquid scintillator provide signals principally from electron antineutrinos, and OMNIS would complement this by providing a large signal from the higher flavours through neutral current excitation of nuclei. In addition, OMNIS can provide a new signal for MSW mixing in the supernova, in the form of a strong two-neutron signal from charged current excitation of lead nuclei by the resulting higher-momentum electron neutrinos.

As currently envisaged, OMNIS would add three new neutrino time profiles to the existing charged and neutral current signals from SuperKamiokande and SNO. These would be

1. single neutron time profile from lead target;
2. single neutron time profile from iron target;
3. two neutron time profile from lead target.

Although the iron target gives fewer events per ton than the lead target, it provides an important comparison material, giving identical mass-dependent effects but free from the two-neutron mixing signal, and would be included in a full scale OMNIS array. Statistical considerations suggest that the OMNIS lead target should be made large enough to provide at least 2000–4000 events from a supernova at 8 kpc, and the iron target at least 1000 events. Division between more than one underground site would be advantageous, for reasons of coincidence and backup. Full interpretation of the $\nu_{\mu,\tau}$ time profile would require comparison with the $\bar{\nu}_e$ profile from other world detectors, but it is also worth noting that OMNIS does contain a useful internal calibration in the form of an additional 3–5% charged current events from direct $\bar{\nu}_e$ interaction in the scintillator. For example an OMNIS array giving 2000 mu/tau neutrino events would also provide 60–100 electron antineutrino events (dependent on the amount of scintillator used to detect the neutron signal). These events are separately identifiable and provide additional confirmation of the start time of the neutrino burst.

Since it is based on well-established materials and technology (lead and iron targets with liquid or plastic scintillator) OMNIS could proceed without significant new development work, and is remarkably efficient in terms of overall size and cost per event. It could also make use of surplus materials from other experiments. Typically the efficient collection of neutrons from nuclear excitation in a lead target allows, for an 8 kpc supernova, the detection of 16 events per ton of scintillator (increasing to 80 events ton^{-1} if MSW mixing occurs). This can be compared with a total 0.7 events ton^{-1} in the planned 1000 ton KamLAND detector [42] (quoted figures scaled to the same supernova distance).

Astrophysical estimates for the time interval between type II/Ib supernovae in our Galaxy are in the range 6 ± 3 per century, consistent with the $\sim$15-year interval estimated specifically from the 2000 year historical record in the local 4–5 kpc sample of the Galaxy. Thus the required (automated) running time would not be dissimilar to that of several past cosmic ray and solar neutrino experiments (20–30 years) or to the timescale for a number of other world neutrino physics and astrophysics programmes currently planned or under construction. A full range of data from a supernova burst would make an important contribution to this, with OMNIS providing the main signal from the higher flavour neutrinos.

Acknowledgements

Valuable discussions with many colleagues are gratefully acknowledged, in particular with G.M. Fuller, G. McLaughlin, D.B. Cline, J.D. Lewin, R.N. Boyd, A. Murphy, E. Fenyves, A. Burrows, G. Raffelt, D. Wark, J. Edgington, I. Liubarsky,

S. Cartwright, V.A. Kudryavtsev, R. Schirato, W. Vernon, K. Lee, R. Marshall, K. Stevens, B. Cox, W.G. Jones, T.W. Jones, F. Boehm, A. Piepke, N.J.C. Spooner, N.J.T. Smith, J. Alner.

References

[1] S.E. Wooseley, et al., Ap. J. 356 (1990) 272.
[2] P.F. Smith, Astropart. Phys. 8 (1997) 27.
[3] D.B. Cline, et al., Nucl. Phys. B 14A (1990) 348.
[4] D.B. Cline, et al., Astro. Lett. Commun. 27 (1990) 403.
[5] D.B. Cline, et al., Phys. Rev. D 50 (1994) 720.
[6] R. Raghavan, Phys. Rev. Lett. 78 (1997) 3618.
[7] R. Raghavan, Proc. Fourth Int. Solar Neutrino Conf., Heidelberg, 1997, p. 248.
[8] P.F. Smith, et al., Proc. Third Int. Dark Matter Conf., Marina del Rey, 1998, p. 465.
[9] P.F. Smith et al., Proc. Fourth Int. Dark Matter Conf., Marina del Rey, in press.
[10] S. Van der Bergh, G. Tammann, Ann. Rev. Astron. Astrophys. 29 (1991) 363.
[11] Y. Totsuka, Rep. Prog. Phys. 55 (1992) 377.
[12] R.G. Strom, Astron. Astrophys. 288 (1994) L1–L4.
[13] P. Dragicevich, D. Blair, R. Burman, Mon. Not. R. Astron. Soc. 302 (1999) 693.
[14] B. Aschenbach, Nature 396 (1998) 141.
[15] K. Hatano, A. Fisher, D. Branch, Mon. Not. R. Astron. Soc. 290 (1997) 360.
[16] G. Raffelt, Stars as Laboratories for Fundamental Physics, Chicago, 1996, p. 395.
[17] H.T. Janka, Proc. Vulcano Workshop, Soc. Ital. Fis. Conf. Proc. 40, 1992.
[18] A. Burrows, Ann. Rev. Nucl. Sci. 40 (1990) 181.
[19] H.A. Bethe, Nucl. Phys. A 606 (1996) 95.
[20] G. Raffelt, personal communication.
[21] J. Bahcall, Neutrino Astrophysics, C.U.P., 1989, p. 442.
[22] M. Koshiba, Phys. Rep. 220 (1992) 229.
[23] P.F. Smith, J.D. Lewin, Phys. Lett. B 127 (1983) 185.
[24] P.F. Smith, J.D. Lewin, Acta Phys. Polon. B 16 (1985) 837.
[25] Y.Z. Qian, et al., Phys. Rev. Lett. 71 (1993) 1965.
[26] G.M. Fuller, B.S. Meyer, Astrophys. J. 453 (1995) 792.
[27] G.M. Fuller, W.C. Haxton, G.C. McLaughlin, Phys. Rev. D 59 (1999) 085005.
[28] C.K. Hargrove, et al., Astropart. Phys. 5 (1996) 183.
[29] E. Kolbe, K. Langanke, preprint nucl-th/0003060 (2000).
[30] E. Kolbe, K. Langanke, Phys. Rev. C, in press.
[31] G.F. Knoll, Radiation Detection and Measurement, Wiley, New York, 1979.
[32] F. Boehm, et al., Nucl. Phys. B (Proc. Suppl.) 77 (1999) 166.
[33] A.G. Piepke, S.W. Moser, V.M. Novikov, Nucl. Instrum. Meth. A 432 (1999) 392.
[34] M. Abbes, et al., Nucl. Instrum. Meth. A 374 (1996) 164.
[35] S. Ait-Boubker, et al., Nucl. Instrum. Meth. A 277 (1999) 461.
[36] S.C. Wang, et al., Nucl. Instrum. Meth. A 432 (1999) 111.
[37] BICRON, Newbury, OH, scintillator product brochure.
[38] Applied Scintillation Technologies, Harlow, UK, data sheets.
[39] M. Bliss, et al., Proc. SPIE 2551 (1995) 108.
[40] G. Drexlin, Nucl. Instrum. Meth. A 329 (1990) 490.
[41] R.N. Boyd, A.St.J. Murphy, Nucl. Phys. A 688 (2001) 386.
[42] A. Suzuki, Nucl. Phys. B (Proc. Suppl.) 77 (1999) 171.
[43] G. Gratta, Y.F. Yang, Nucl. Instrum. Meth. A 438 (1999) 317.
[44] L.-S. The, et al., Proc. Ringberg Castle Workshop Astronomy and Radioactivity, September 1999, p. 77.
[45] T.K. Kuo, J. Pantaleone, Phys. Rev. D 37 (1988) 298.
[46] J.F. Beacom, R.N. Boyd, A. Mezzacappa, Phy. Rev. Lett. 85 (2000) 3568.
[47] F.T. Avignone, R.L. Brodzinski, Prog. Part. Nucl. Phys. 21 (1988) 99.
[48] J.H. Reeves, et al., IEEE Trans. Nucl. Sci. NS-31 (1984) 697.